Original Paper

Tempering glass spheres and related topics

O. S. Narayanaswamy
Dearborn Heights, MI (USA)

Robert Gardon
Farmington Hills, MI (USA)

The generation of permanent stresses in glass spheres by rapid cooling is described, starting with transient stresses that arise during the tempering process. The utility of tempered glass spheres is briefly considered in the context of the permanent stresses produced. Two possible effects of transient stresses are: the risk of in-process breakage as a result of excessive tension in an already cold surface, and bubble formation in – or other distortion of – spheres as a result of high hydrostatic tension in their interior while that is still hot and fluid. In that connection, the distortion of the edges of tempered glass plates is also briefly considered. The mathematical model of tempering spheres, on which this discussion is based, is outlined in an appendix.

Vorspannen von Glaskugeln und verwandte Themen

Die durch schnelles Abkühlen bedingte Erzeugung von dauerhaften Spannungen in Glaskugeln wird beschrieben, angefangen bei kurzzeitigen, während des Vorspannens entstehenden Spannungen. Der Nutzen von vorgespannten Glaskugeln wird im Hinblick auf die dauerhaft erzeugten Spannungen kurz dargestellt. Zwei mögliche Auswirkungen von kurzzeitigen Spannungen sind die Gefahr von Bruch während der Fertigung aufgrund von übermäßiger Spannung in einer schon abgekühlten Oberfläche, sowie die Bildung von Blasen – oder anderen Verformungen – in Glaskugeln aufgrund hoher hydrostatischer Spannung in ihrem Inneren, während dieses noch heiß und flüssig ist. In diesem Zusammenhang wird auch die Verformung der Kanten von vorgespannten Flachglasscheiben kurz betrachtet. Im Anhang der Arbeit findet sich ein Abriß des mathematischen Modells für das Vorspannen von Glaskugeln, auf dem die Untersuchung beruht.

1. Approach

The authors' approach to modeling the process of tempering glass spheres is based on the idea of "instant freezing", first introduced by Bartenev [1]. Accordingly, glass is treated as a perfect fluid having zero viscosity ($\eta = 0$) above an empirically determined "glass (transition) temperature", T_g and as an elastic solid ($\eta = \infty$) below this temperature. This approximation is made useful – for rapidly chilled bodies of glass – by the very rapid rise in the viscosity of all glasses with decreasing temperatures.

Bartenev proposed a heuristic model of instant freezing to calculate residual stresses in a tempered glass plate. Later Indenbom [2] presented a rigorous analysis of this problem based on the three fundamental principles of stress analysis: first, the compatibility of strains, second, the equilibrium of stresses and third, a constitutive relation connecting stresses and strains. The present model of tempering glass spheres embodies these same basic principles. However, it also deals with an aspect of the "instant freezing model" not encountered in earlier work on tempered plates. This is discussed in section 7.1. The derivation of the relevant equations will be found in section 7.2.

Received January 27, revised manuscript September 3, 1997.

In line with the classic "instant freezing" approach, it is assumed that a sphere at an initial temperature T_0 is subjected to quenching in a cooling medium having a temperature T_C and a heat transfer coefficient h. Both T_C and h are taken to be uniform over the surface of the sphere and to remain constant until the center of the sphere has cooled to T_g. During this time, a "freezing front" will have migrated from the surface to the center, and some stresses will have been generated throughout the sphere, which is now solid and elastic. Stresses continue to develop as the sphere approaches room temperature and the temperature distribution existing at the end of solidification decays. The manner of cooling during this last stage is immaterial.

In the past, the instant freezing model was used to predict residual, i.e. permanent, stresses only. With an appropriate choice of physical properties and process parameters, such predictions for tempered glass plates are known to be very good. In the present work, the authors are adapting the instant freezing model to spheres and also using it to calculate transient stresses.

Since the work of Bartenev and Indenbom, other, more comprehensive models of the generation of stresses in glass have been developed [3 to 8]. These take account of viscoelasticity and the glass transition, so that they are applicable to a wider range of process conditions;

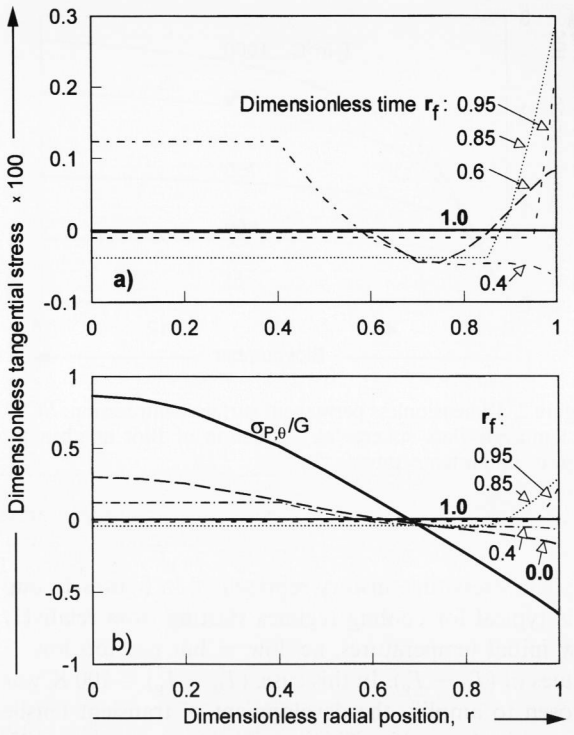

Figures 1a and b. Radial distribution of dimensionless tangential stresses, σ_θ/G, in a tempered glass sphere, cooled from T_0 = 650 °C, with Bi = 8; a) transient stresses during initial stages of tempering, b) transient stresses during tempering and the permanent stresses produced. $\sigma_{P,\theta}/G$ are the permanent tangential stresses, attained in an isothermal sphere at room temperature.

indeed, to annealing as well as tempering. They are also better suited for tracking transient stresses. However, their application to spheres would have entailed much more work, and the use of the "instant freezing" model was deemed adequate for this first look at the tempering of glass spheres. A further simplification was made by not explicitly taking account of thermal radiation, using instead an "effective" thermal conductivity of the glass [9]. These simplifications yielded results that afford a good overview of the subject: With fewer variables involved, the results can readily be generalized by being cast in dimensionless form.

2. Results

2.1 General

The results of the analysis presented themselves in terms of two dimensionless variables:

a) The Biot number, Bi, encompasses the variables affecting the rate of cooling the glass

$$Bi = (R \cdot h)/k \ .$$

b) The dimensionless stress takes the form

$$\sigma/G \ ,$$

where G = shear modulus of the glass, and σ = stress. This may be radial or tangential, transient i.e. a function of time and position in the sphere, or permanent i.e. a function of position only – as indicated in context and by subscripts. The temperatures T_0, T_g and T_C are kept dimensional.

2.2 Range of variables considered

Where quantitative results are given, they assume that the spheres are made of a glass substantially similar to plate glass, with properties as given below. Some data on heat transfer coefficients that may be involved are included.

a) Properties of plate glass

G = shear modulus
= 27 GPa (at room temperature)
[= $3.9 \cdot 10^6$ psi],

k = "effective" thermal conductivity
= 1.3 W/(m · K)[1] [= 0.003 cal/(cm · s · K)],

$c\varrho$ = volumetric specific heat
= 2.5 MJ/(m³ · K) [= 0.6 cal/(cm³ · K)],

T_g = "glass temperature" = 550 °C,

β_g = coefficient of expansion of ("solid") glass
= $11.2 \cdot 10^{-6}$ K^{-1},

$\beta_{s,eff}$ = assumed "effective" structural expansivity = β_g (see section 6.1),

ν = Poisson's ratio = 0.22.

b) Heat transfer coefficients

Orders-of-magnitude of the heat transfer coefficients that may be of interest here are:

h: for natural convection in air
≈ 13 W/(m² · K) [= 0.0003 cal/(cm² · s · K)],

h: for forced convection in air
≈ 0.13 – 1.3 kW/(m² · K)
[= 0.003 – 0.03 cal/(cm² · s · K)],

h: for quenching in water
≈ 6.3 kW/(m² · K) [= 0.15 cal/(cm² · s · K)].

The temperature of the cooling medium, T_C, is taken as 100 °C.

2.3 Generation of stresses – Transient stress profiles

To begin with, it will be illustrated how stresses arise in the course of tempering a sphere under a particular set of conditions. Figures 1a and b apply to a sphere, cooled with Bi = 8 from an initial temperature of 650 °C. They are plots of dimensionless tangential stresses versus dimensionless position r within the sphere (r = 0 at the center, r = 1 at the surface), drawn for different "times". Positive and negative stresses denote tension and compression, respectively. Time is represented in dimensionless form by the corresponding position r_f of the

[1] This is approximately 1.5 times the "true" thermal conductivity, reflecting the fact that radiation plays only a secondary role when glass is rapidly quenched. For simplicity's sake k was also taken as independent of process conditions and the size of spheres.

"freezing front", and it increases as r_f runs from 1 to 0. These curves therefore apply to all spheres, regardless of size, that are cooled from 650 °C with $Bi = 8$. (To put this in concrete, dimensional terms, these plots may be thought of applying to a 3.2 mm diameter sphere quenched in water ($h = 6.3$ kW/(m^2 K)) or to a 96 mm sphere cooled by forced convection in air ($h = 0.2$ kW/(m^2 K)). The actual time intervals between $r_f = 1$ and $r_f = 0$ for these two cases are 0.5 and 450 s, respectively.)

Figure 1a illustrates the initial stages of cooling, at first the surface and then layers of glass close to the surface "freeze". As a progressively thicker outer shell of the sphere becomes "solid", tensile stresses in the surface increase. For "times" of $r_f = 0.95$ and $r_f = 0.85$, tensile forces in the solid outer shell are balanced by hydrostatic compression in the fluid interior that is, as it must be, uniform throughout the interior. As the freezing front penetrates beyond $r = 0.85$, tension in the surface diminishes, and the shape of stress distributions changes. This is illustrated for the "time" $r_f = 0.6$. Now tensile forces in the outermost layers are balanced, for the most part, by compression in the solid layers nearer the freezing front. Hydrostatic compression of the interior is correspondingly reduced. As time progresses, all of the solid region near the surface goes into compression and the hydrostatic stress in the interior changes to tension, as shown by the curve for $r_f = 0.4$.

It is interesting to note that – for comparable conditions of cooling – the shape of transient stress profiles in plates resembles that for $r_f = 0.6$ in figure 1a, rather than that for $r_f \geq 0.85$. The reason for this is that, in a sphere, the fluid interior is confined within a solid shell, so that the interior can support hydrostatic tension or compression. Both kinds of stress profile are therefore possible. In plates, on the other hand, the fluid interior is not confined, so that it cannot sustain stresses. Tension in solid layers near the surface of a plate can therefore be balanced only by compression in solid layers further from the surface. Matters are somewhat different at the edges of a plate, which freeze as soon as the surfaces. This will be touched upon later.

Figure 1b shows stresses from the solidification of the surface, through solidification of the center, to the attainment of isothermal conditions at room temperature. On this scale, the phenomena illustrated in figure 1a barely show up. But figure 1b also shows the curve for $r_f = 0$, which corresponds to the time at which the freezing front reaches the center of the sphere. The further development of stresses is due to the decay of temperature gradients in the now wholly elastic sphere, and the curve labeled $\sigma_{P,\theta}/G$ represents the final and permanent radial distribution of tangential stresses in the sphere. For this particular combination of Biot number and $(T_0 - T_g)$, about a third of the permanent surface stress arose during solidification of the sphere, and two thirds during the subsequent stage of temperature equalization.

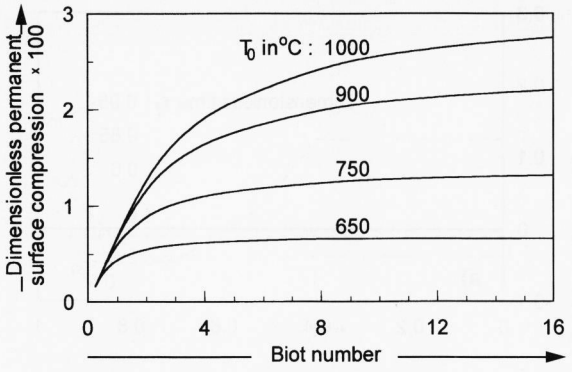

Figure 2. Dimensionless permanent surface compression, *SC/G*, in tempered glass spheres as a function of Biot number, for various initial temperatures, T_0.

The stress-time history represented in figures 1a and b is typical for cooling regimes starting from relatively low initial temperatures, i.e. low – but not too low – values of $(T_0 - T_g)$. In this case, $(T_0 - T_g) = 100$ K was chosen to amplify the development of transient tensile stresses in the surface. Their maximum, at time $r_f = 0.85$, is $0.0029 \cdot G$, i.e. 78 MPa (or 11 000 psi). Transient tensions in the surface of this magnitude pose a small risk of in-process breakage; although, of course, it is well known that, if glass is quenched from initial temperatures that are too low, the danger exists that it may fracture as a result of excessive transient tensile stresses in the surface, or an edge [1 and 5]. More typically, quenching from higher initial temperatures avoids transient tensions in the surface altogether: The surface then goes directly into compression (see curve for $\beta_{s,eff}/\beta_g = 1$ in figure 8a), and hydrostatic stresses in the still liquid part of the sphere are tensile at all times.

2.4 Permanent stresses as a function of process parameters

Tempered glass is of technical interest mainly because high compressive stresses in its surface enhance its strength. For some application it is also important that, if broken, tempered glass breaks into small, blunt – and therefore harmless – particles. This latter characteristic is attributable to high tensile stresses in its interior [10 and 11]. Having considered how temper stresses arise, it will be next considered how their magnitude and distribution depend on process parameters.

2.5 Surface compression

Figure 2 shows the dimensionless permanent surface compression (*SC/G*) as a function of Biot number, for various initial temperatures, T_0. These were chosen somewhat arbitrarily: 650 and 750 °C for larger, manually formed spheres; 900 and 1000 °C perhaps being applicable for very small spheres, formed from drops of liquid glass by surface tension and immediately

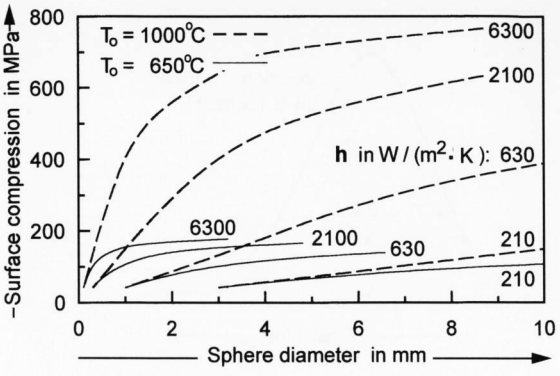

Figure 3. Permanent surface compression as a function of sphere diameter and heat transfer coefficient, h, for initial temperatures, T_0, 1000 and 650 °C.

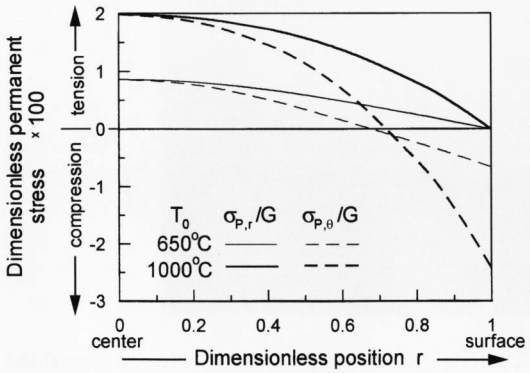

Figure 4. Radial distribution of dimensionless permanent stresses, σ_P/G, in tempered glass spheres. Bi = 8, T_0 in °C.

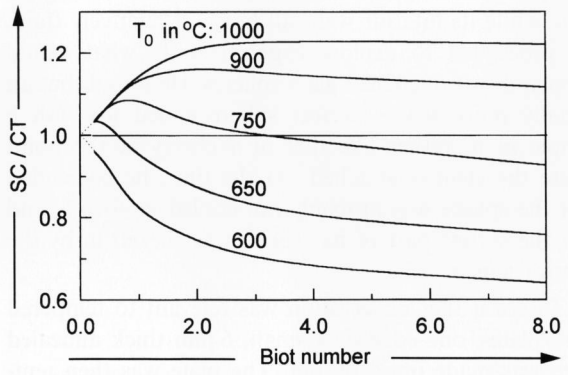

Figure 5. Ratio of the permanent surface compression, SC ($= -\sigma_{P,\theta}$ at $r = 1$), to center tension, CT ($= \sigma_{P,\theta} = \sigma_{P,r}$ at $r = 0$), as a function of Bi and T_0.

quenched. The figure shows that – except for the lowest Biot numbers, i.e. cooling rates – temper stresses diminish as the initial temperature is reduced.

Figure 3 shows some of the same results in dimensional form, i.e. the permanent surface compression SC, in MPa, as a function of sphere diameter for various heat transfer coefficients, h, and initial glass temperatures, T_0. Note that not all combinations of the implied process parameters are useful or even feasible. Thus, for example, cooling 0.5 mm spheres from 1000 °C in air produces uninterestingly low stresses, while quenching them in water (h = 6.3 kW/(m^2 K)) should produce surface compressions of the order of 300 MPa (45 000 psi). On the other hand, much larger spheres can neither be brought to so high an initial temperature without risking deformation, nor quenched in water without risk of fracture. For these T_0 is more likely to be 650 °C, h < 1.3 kW/(m^2 K), and temper stresses about 100 MPa.

Prince Rupert's drops are formed by quenching large drops of liquid glass in water. In falling, they assume their characteristic tear-drop shape, with a long tail. As a result of changing shape and of not being quenched uniformly, their liquid cores are not confined from the onset of the solidification of the surface. Permanent stresses in them will therefore be lower than would be calculated for a sphere having a diameter equal to their bulbous end. Figure 3 suggests that such spheres, 6 to 10 mm in diameter, might have a surface compression of about 750 MPa (110 000 psi), which may be regarded as an upper bound of the surface compression in Prince Rupert's drops. Indeed, a recent paper [12] reported measured surface compressive stresses of 90 to 170 MPa. If anything, they seem surprisingly low – of the same order as surface stresses in tempered automotive glass. Yet, fragile though the tails of Prince Rupert's drops may be, their bulbs cannot be broken with a hammer.

To put these results into perspective: In small glass spheres, 0.5 to 1 mm in diameter, such as are used for shot peening, it should be possible to produce a surface compression of 300 to 400 MPa. This may make them as strong as the bulbs of Prince Rupert's drops. In any case, it represents a significant enhancement of their strength, bearing in mind that the surface compression in tempered automotive glass is only about 100 MPa. Tempering may also enhance the abrasion resistance of small spheres on account of the greater density of the (compressed) surface layers.

2.6 Stress distributions

The radial distribution of both radial and tangential permanent stresses is shown in figure 4 for Bi = 8 and for two representative values of T_0. Note that radial stresses vanish at the surface of a sphere; while, near its center, radial and tangential stresses are nearly equal. At the center they are perfectly hydrostatic.

Figure 5 shows the ratio of surface compression and center tension as a function of Biot number and initial glass temperature. For all but the lowest initial temperatures, this ratio at first increases with Bi, passes through a maximum and then levels off – at about 1.2 for T_0 = 1000 °C and less than 1.0 for 750 °C. This is in marked contrast with the corresponding ratio for plates, which is exactly 2 for annealed plates (i.e. for plates that are cooled very slowly) and about 2.2 for tempered plates, increasing slightly for higher rates of quenching [5]. This means that, for a given surface compression,

the center tension is higher in spheres than it is in plates; which, in turn, suggests that the propensity of tempered spheres to break into fine particles is greater than that of tempered plates.

2.7 Bubble formation as a result of tempering?

For all but the lowest initial temperatures, surface stresses are compressive virtually throughout the tempering process (see curves for $\beta_{s,eff}/\beta_g \geq 1$ in figures 8a and b). Correspondingly, hydrostatic stresses in the still fluid interior are tensile at all times. This prompts the question whether such tension may cause the nucleation of bubbles in the glass. For a given composition of glass and concentration of nucleation sites and dissolved gases, one might expect that nucleation would be the more probable the more the hydrostatic tension exceeds the partial pressure of dissolved gases, the hotter and less viscous the glass, and the longer the time available.

Even without information on partial pressures, the authors tried to give this hypothesis a tentative quantitative form. For this they defined a "flow number", ϕ, as the product of the local hydrostatic tension and the local fluidity ($1/\eta$). Figure 6 is a schematic representation of ϕ as a function of real time for various positions in the interior. The probability of bubble formation, as a result of tempering, in a glass sphere having a uniform distribution of nucleation sites would then be expected to be governed by the area under the ϕ versus time curves. This area is seen to be highest for the center ($r = 0$). It would be higher still for spheres of the same size quenched more rapidly, and it vanishes for positions $r > 0.6$. Without relevant experimental data, this remains a speculation for now.

Bubbles are a common occurrence in Prince Rupert's drops. Their formation may involve some mechanism such as that indicated by figure 6; although, of course, the temperature- and stress-history of Prince Rupert's drops is more complex than that of spheres. In the course of this work the authors also learned of decorative glass spheres containing bubbles. These spheres are made of a glass so full of nucleation sites and so highly saturated with gases that even very gentle cooling brought about the formation of bubbles. Indeed, once bubbles started to appear, the spheres were annealed to prevent breakage. The process resembles annealing with variable cooling rates, which cannot be analyzed by the present "instant freezing" approach. It could be treated, as indeed a variety of annealing schedules were treated [13 and 14], by taking proper account of the viscoelastic and structural relaxation processes involved. These are involved in both annealing and tempering; but they can be approximated by the instant freezing approach only in the case of tempering, not the very much slower process of annealing.

3. Other effects of transient internal tension

Many years ago, when he started his study of tempering glass plates, one of the authors (R. Gardon) was intrigued by the notion of tension in the interior of a glass plate while its interior was still hot and relatively fluid. He proceeded to explore experimentally what would happen if one quenched glass spheres. He found that an initially more-or-less perfect sphere ended up with a dimple in it, rather like that in a cherry at the point where the stem is attached. At the time, he concluded that the sphere was probably not cooled uniformly and that the softest part of its "shell" was sucked in by the interior tension.

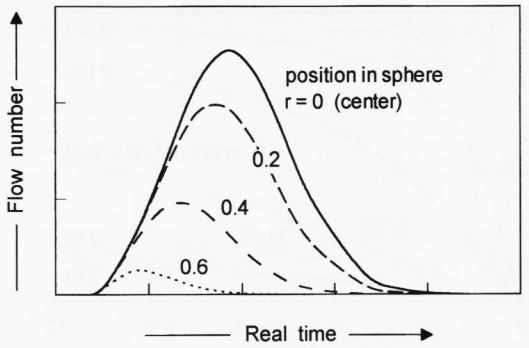

Figure 6. Schematic representation of the flow number, ϕ, as a function of time for various radial positions in a sphere.

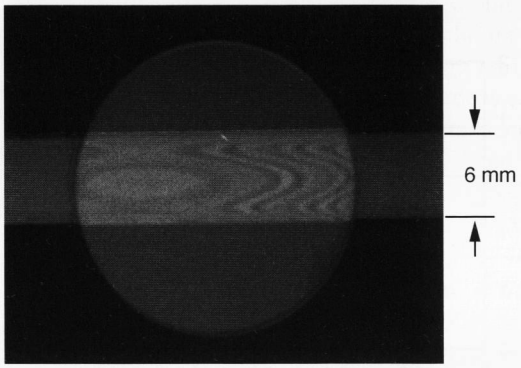

Figure 7. Interference fringes produced between an optical flat and the 6 mm wide edge of a tempered glass plate. The edge was optically flat before tempering.

To see if that observation was relevant to tempered glass plates, one edge of a small, 6 mm thick annealed plate was made optically flat. The plate was then tempered and its edge examined again. It was found to be minutely deformed, as shown in the interferogram of figure 7. This suggests a central longitudinal depression along the edge – perhaps analogous to a dimple in a sphere – with ridges on both sides, about 1 mm inboard of the principal surfaces of the plate. This configuration results from an interesting interplay of transient stresses in the edge region.

When a glass plate is tempered, its principal surfaces and edges "solidify" first. Initially, the surfaces also contract more rapidly than the interior. This would tend to put the still "fluid" interior under compression. Two other factors tend to put the interior under tension:

First, the expansion coefficient of the liquid is three times higher than that of solid glass; and, second, the rate of cooling of interior layers begins to exceed that of outer layers while the former are still above T_g. In fact, far from edges of the plate, where there is no resistance to the movement of the solid outer layers in the normal direction, the fluid core will not sustain any stress, because it can maintain its desired volume. Matters are different near the edges, where movement of the outer layers is restricted. Adjacent regions of the fluid core are thus more-or-less confined. The resulting average pressure or tension in these regions causes a distortion of the initially flat edge, which – though "solid" in the loose terminology of the instant freezing model – is still deformable.

It would seem that, starting the quench from a high enough initial temperature, the edge bulges outward during the first instants of solidification. A very short while later, the average stress in the confined region of the still fluid core changes to tension. This tends to pull the edge inward, but – since the edge has meanwhile cooled some more – only a narrower, central strip responds. The profile of the tempered edge shown in figure 7 thus results from the superposition of a narrow, central depression on an earlier bulge that spans the entire width of the edge.

The authors now recognize that "dimpling" could occur even if cooling was ideally uniform over the surface of the sphere. Which of the two phenomena – bubble formation or dimpling – comes into play may well be determined by the relative rates of increase of the thickness (or stiffness) of the cold outer shell and of tension in the still fluid interior. Alternatively, it may also happen – as for example in glass with a low concentration of dissolved gases – that neither of the above two phenomena occurs.

4. Summary

The authors have considered both the permanent stresses produced by tempering glass spheres and the transient stresses that arise in the course of that process. For their analysis, they extended the classical "instant freezing" model of tempering by making some allowance for partial relaxation of stresses of structural origin, which is negligible in tempering glass plates but significant in the case of spheres.

The principal findings of this analysis are:

a) Apart from the physical properties of the glass, the permanent stresses produced in a tempered glass sphere depend primarily on $(T_0 - T_g)$ and the Biot number $(Bi = (R \cdot h)/k)$ with which the sphere is quenched.

b) The variables R, h or k, individually, affect only the time scale of the solidification of a glass sphere, which – in turn – governs the time dependence of transient stresses.

c) If one defines a new time scale in terms of when successive layers (shells) in the sphere solidify, then transient stresses also come to depend only on Bi, and not on R, h or k individually.

d) The probability of fracture during tempering is governed by the largest transient tensile stress in the surface, regardless of when during solidification it occurs.

e) Bubble formation in and distortion of a sphere were also considered, which depend on transient stresses in a more complex manner.

f) Finally, the genesis and distribution of temper stresses in spheres and plates are briefly compared.

5. List of symbols

Bi	Biot number $= (R \cdot h)/k$
c	specific heat capacity of glass in J/(kg K)
$c\varrho$	volumetric specific heat capacity of glass in J/(m^3 K)
CT	permanent center tension in a tempered sphere, i.e. $\sigma_{P,r}$ at $r = 0$ in Pa
G	shear modulus of glass (at room temperature) in Pa
h	heat transfer coefficient for quenching glass in W/(m^2 K)
k	"effective" thermal conductivity of glass in W/(m K)
K	bulk modulus of glass (at room temperature) in Pa
p	pressure in Pa
r	non-dimensional radial coordinate, 0 at the center of the sphere and 1 at its surface
r_f	a dimensionless measure of time, corresponding to the passage of the "freezing front" through the position r. This time runs from 1 to 0.
$(1 - r_f)$	an aesthetically more pleasing "dimensionless time" that runs from 0 to 1
R	radius of sphere in m
SC	permanent surface compression in a tempered sphere, i.e. $-\sigma_{P,\theta}$ at $r = 1$ in Pa
t	time in s
T	temperature in °C
T_C	temperature of coolant in °C
T_g	glass (transition) temperature in °C
T_0	initial temperature of glass in °C
α_n	n-th root of the trigonometric equation $(\alpha \cdot \cot \alpha + Bi) = 1$
β	coefficient of expansion (β_g of (solid) glass, β_l of liquid glass) in K^{-1}
β_s	$= (\beta_l - \beta_g)$ = structural expansivity
$\beta_{s,eff}$	assumed "effective" structural expansivity (see section 7.1)
γ	actual maximum shear strain, from all sources of deformation. Its sources are distinguished by the subscripts "e" for elastic and "v" for viscous.
ε	actual bulk strain from all sources of deformation
ε_r, ε_θ	actual radial (subscript r) and tangential (subscript θ strains. The sources ε, ε_r and ε_θ are distinguished by the subscripts "e" for elastic and "th" for thermal.
η	viscosity of glass in Pa s
ν	Poisson's ratio of glass
ϱ	density of glass in kg/m^3
σ	stress in Pa. Without a subscript, σ refers to a transient stress, i.e. a function of time and position in the sphere.
σ_P	permanent stress, i.e. a function of position only
σ_r, σ_θ	radial or tangential stress. Also, in context, $\sigma = (1/3) \cdot (\sigma_r + 2\sigma_\theta)$ = average stress $= -p$
τ	$(\sigma_r - \sigma_\theta) = 2 \cdot$ (maximum shear stress) in Pa

6. References

[1] Bartenev, G. M.: Tempering of glass. (Orig. Russ.) Zh. Tekh. Fiz. **19** (1949) no. 12, p. 1423–1433.

[2] Indenbom, V. L.: Theory of tempering glass. (Orig. Russ.) Zh. Tekh. Fiz. **24** (1954) no. 5, p. 925–928.

[3] Gardon, R.; Narayanaswamy, O. S.: Stress and volume relaxation in annealing flat glass. J. Am. Ceram. Soc. **53** (1970) no. 7, p. 380–385.

[4] Narayanaswamy, O. S.: Stress and structural relaxation in tempering glass. J. Am. Ceram. Soc. **61** (1978) no. 3–4, p. 146–152.

[5] Gardon, R.: Thermal tempering of glass. In: Uhlmann, D. R.; Kreidl, N. J. (eds.): Glass: Science and Technology. Vol. 5. New York (et al.): Acad. Press, 1980. p. 145–216.

[6] Narayanaswamy, O. S.: Annealing of glass. In: Uhlmann, D. R.; Kreidl, N. J. (eds.): Glass: Science and Technology. Vol. 3. Orlando (et al.): Acad. Press, 1986. p. 275–318.

[7] Gardon, R.: Evolution of theories of annealing and tempering: historical perspective. Am. Ceram. Soc. Bull. **66** (1987) no. 11, p. 1594–1599.

[8] Mauch, F.; Jäckle, J.: Thermoviscoelastic theory of freezing stress and strain in a symmetrically cooled infinite glass plate. J. Non-Cryst. Solids **170** (1994) p. 73–86.

[9] Gardon, R.: A review of radiant heat transfer in glass. J. Am. Ceram. Soc. **44** (1961) no. 7, p. 305–312.

[10] Acloque, P.: Influence de l'état de contrainte du verre sur les modalités de sa fracture. In: Travaux IV^{e} Congrès International du Verre, Paris 1956. p. 279–291.

[11] Fayet, A.; Guillemet, C.; Acloque, P.: Dynamic study of the shape of the fracture front in the thickness of a tempered glass plate. In: Nilsson, N. R.; Högberg, L. (eds.): Proc. 8th International Congress on High Speed Photography, Stockholm 1968. p. 433–434.

[12] Chandrasekar, S.; Chaudry, M. M.: The explosive disintegration of Prince Rupert's drops. Phil. Mag. **B70** (1987) no. 6. p. 1195–1218.

[13] Gardon, R.: Nonlinear annealing of glass. J. Am. Ceram. Soc. **64** (1981) no. 2, p. 114–119.

[14] Gardon, R.: Modelling annealing lehrs for flat glass. J. Am. Ceram. Soc. **65** (1982) no. 8, p. 372–379.

[15] Gardon, R.: Variation of densities and refractive indices in tempered glass. J. Am. Ceram. Soc. **61** (1978) no. 3–4, p. 143–146.

[16] Carslaw, H. S.; Jaeger, J. C.: Conduction of heat in solids. Oxford: Univ. Press, 1947.

7. Appendices

7.1 Allowing for partial relaxation of structurally induced stresses in an IFM

As was noted in section 1., the application of the "Instant Freezing Model" (IFM) to spheres presented a problem not encountered with plates. Instant freezing implies that, once the surface of a sphere is frozen, its liquid core is confined and thus capable of supporting hydrostatic stresses. With the liquid core under stress, account must be taken of the fact that liquid glass has a much higher coefficient of thermal expansion than the solid outer shell. Viscoelastic models of stress analysis allow for a partial relaxation of stresses that arise from such structural heterogeneity. The IFM, by contrast, cannot comprehend partial stress relaxation: By definition, stress relaxation must be either complete or nonexistent.

The "structural expansivity", β_s, is the difference between the expansion coefficients of liquid and solid glass, respectively, i.e $(\beta_l - \beta_g)$. It has been shown to be equal to about $2\,\beta_g$. Using this physically correct value of the structural expansivity in an IFM would lead to a full build up of stresses of structural origin without allowing for any relaxation. Using $\beta_s = 0$ would suppress all effects of the different expansivities of liquid and solid glass, which would be tantamount to complete relaxation

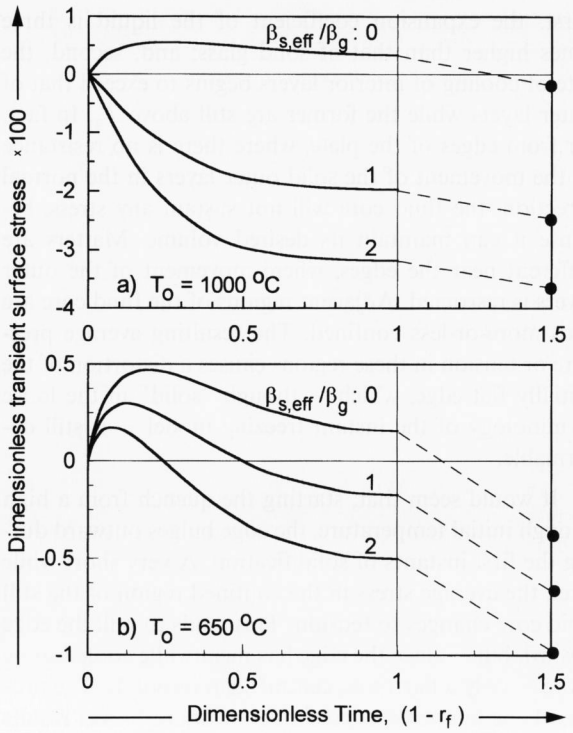

Figures 8a and b. Dimensionless stresses in the surface of a tempered sphere, σ_θ/G at $r = 1$, as calculated by the instant freezing model using various assumptions regarding the value of the effective structural expansivity, $\beta_{s,eff}$; drawn for T_0 of 1000 (figure a) and 650 °C (figure b). Solidification occurs from $(1 - r_f) = 0$ to 1. Permanent stresses are arbitrarily shown at 1.5.

of structurally induced stresses. The compromise of taking $\beta_{s,eff} = \beta_g$ should allow the IFM to simulate partial relaxation of structurally induced stresses and yield realistic results. Needless to say, there is nothing sacrosanct about taking $\beta_{s,eff}/\beta_g$ equal to 1. One could equally well have assumed it to be 0.8 or 1.3. (This issue could be handled rigorously by taking proper account of the stress- and structural-relaxation processes involved in generating permanent stresses in glass. The authors discuss in [3 to 6] the dominant temperature-and-time-dependence of these relaxation processes as they affect the tempering and annealing of glass plates. Mauch and Jäckle [8] extended these analyses by also taking account of the pressure-and-time-dependence of relaxation. While this probably plays only a minor role in tempering plates, it may well be more significant in tempering spheres, in which larger pressures come into play because their interiors are confined.)

Figures 8a and b show how the assumed value of $\beta_{s,eff}$ affects the calculated course of the development of stresses in the surface of a sphere. They are plots of dimensionless stresses (σ_θ/G) in the surface of a sphere as a function of dimensionless time, now represented as $(1 - r_f)$, r_f being the time at which the freezing front passes through the radial position r within the sphere. Thus, stresses at times from 0 to 1 are transient surface stresses during solidification of the sphere. The dimensionless permanent surface stress $(\sigma_{P,\theta}/G)$, attained when the entire sphere has reached room temperature, is arbitrarily shown at time = 1.5.

Figure 8a, for an initial temperature of 1000 °C, shows that taking $\beta_{s,eff}/\beta_g$ as 1 or 2 gives qualitatively similar results: The surface is under compression, and therefore the interior under tension, throughout the tempering process. This is a plausible result and not strongly dependent on the precise value of $\beta_{s,eff}$.

It is also in marked contrast with results produced by the less plausible assumption of $\beta_s = 0$, which would correspond to total structural relaxation.

As figure 8b shows, the choice of an effective value of β_s is more critical for low initial temperatures, such as 650 °C. As before, $\beta_{s,eff} = 0$ is a totally unrealistic assumption. But now the choice between $\beta_{s,eff}/\beta_g$ equaling 1 or 2 has a proportionately greater effect on both transient and permanent stresses, and it also affects the proportion of time, during tempering, that the still fluid interior is under compression. The predicted propensity for bubbles to form as a result of tempering would clearly increase as $\beta_{s,eff}$ approaches $2\,\beta_g$, i.e. as the method of calculation, using this modified IFM, allows for less relaxation of structurally induced transient stresses.

Structural heterogeneity also exists in tempered glass plates [15], but this is due mainly to the slightly different expansivities of regions of solid glass cooled at different rates. The very much bigger difference between the expansivities of liquid and solid glass is irrelevant because, as was discussed earlier, the fluid core of a plate is stress-free during tempering, since it is free to adjust its volume by changing its thickness.

7.2 The instant freezing model of tempering glass spheres

For a point of departure see section 1. The following derivation of equations is unaffected by section 7.1, which deals only with the choice of an appropriate value of $\beta_{s,eff}$. In equations (13a and b), therefore, $\beta_{l,eff} = \beta_g + \beta_{s,eff}$ is used instead of β_l, the true thermal expansion coefficient of liquid glass.

The constitutive relation, being a material property, is the same for a plate or a sphere. For the instant freezing model, this relation is

$$\gamma_e = \varepsilon_{re} - \varepsilon_{\theta e} = (1/2) \cdot \tau/G = 0 \qquad \text{for } \eta = 0 \text{ and } T \geq T_g, \tag{1a}$$

$$\gamma_e = \varepsilon_{re} - \varepsilon_{\theta e} = (1/2) \cdot \tau/G \qquad \text{for } \eta = \infty \text{ and } T < T_g, \tag{1b}$$

and

$$\varepsilon_e = \sigma/K. \tag{1c}$$

For spherically symmetric cooling, the compatibility of radial and tangential strains is given by

$$\frac{d\varepsilon_\theta}{dr} - \frac{\varepsilon_r - \varepsilon_\theta}{r} = 0 \tag{2}$$

and the equilibrium of stresses by

$$\frac{d\sigma_r}{dr} + 2\,\frac{\sigma_r - \sigma_\theta}{r} = 0\,. \tag{3}$$

The surface of the sphere must always be free of radial stress, yielding the boundary condition:

$$\sigma_r(1) = 0\,. \tag{4}$$

Since the constitutive equations (1a to c) are given in terms of shear and bulk components of stress and strain, it is advantageous to cast the compatibility and equilibrium equations in the same form. The actual shear (γ) and bulk (ε) strains are therefore expressed as sums of their respective thermal, elastic and viscous strain components. Noting that the thermal shear strain $\gamma_{th} = 0$ and the viscous bulk strain $\varepsilon_v = 0$, it may be written:

$$\gamma = \gamma_e + \gamma_v \tag{5a}$$

and

$$\varepsilon = \varepsilon_{th} + \varepsilon_e\,. \tag{5b}$$

By definition, the shear and bulk strains are

$$\gamma = \varepsilon_r - \varepsilon_\theta \tag{6a}$$

and

$$\varepsilon = \varepsilon_r + 2\,\varepsilon_\theta\,. \tag{6b}$$

Inversion of equations (6a and b) yields

$$\varepsilon_r = (1/3) \cdot (\varepsilon + 2\,\gamma) \tag{7a}$$

and

$$\varepsilon_\theta = (1/3) \cdot (\varepsilon - \gamma). \tag{7b}$$

Expressions similar to equations (7a and b) are obtained for radial and tangential stresses from definitions of the shear stress (τ) and average stress (σ) given earlier. Thus

$$\sigma_r = \sigma + (2/3) \cdot \tau \tag{8a}$$

and

$$\sigma_\theta = \sigma - (1/3) \cdot \tau\,. \tag{8b}$$

The compatibility condition is recast by substituting equations (5a and b) in equations (7a and b), which, in turn, are substituted in equation (2), yielding

$$\frac{d\varepsilon_e}{dr} - \frac{d\gamma_e}{dr} - 3\,\frac{\gamma_e}{r} = -\frac{d\varepsilon_{th}}{dr} + \frac{d\gamma_v}{dr} + 3\,\frac{\gamma_v}{r}\,. \tag{9a}$$

The equilibrium equation (3) is rewritten using equations (8a and b) and the elastic constitutive relations of equations (1b and c), yielding

$$\frac{d\varepsilon_e}{dr} + \frac{4}{3}\,\frac{G}{K}\,\frac{d\gamma_e}{dr} + 4\,\frac{G}{K}\,\frac{\gamma_e}{r} = 0\,. \tag{9b}$$

Subtracting equation (9a) from equation (9b) and introducing the following auxiliary shear strain variable,

$$\gamma_{aux} = \left(1 + \frac{4\,G}{3\,K}\right)\gamma_e + \gamma_v \tag{10}$$

yields a simple linear differential in the unknown γ_{aux}. It is

$$\frac{d\gamma_{aux}}{dr} + 3\,\frac{\gamma_{aux}}{r} = \frac{d\varepsilon_{th}}{dr}\,. \tag{11}$$

Applying an integrating factor of r^3 permits one to obtain the following integral of equation (11)

$$\gamma_{aux} = \frac{1}{r^3}\int_0^r (r')^3\,\frac{d\varepsilon_{th}}{dr'}\,dr'\,. \tag{12}$$

It is clear from equations (11 and 12) that the thermal strain gradient is the driving force in this problem. It generates elastic and viscous strains, which in turn produce transient and permanent stresses in the glass sphere. The thermal strain itself is given by

$$\varepsilon_{th} = \beta_l \cdot (T - T_0) \qquad \text{for } T \geq T_g \text{ and} \tag{13a}$$

$$\varepsilon_{th} = \beta_l \cdot (T_g - T) + \beta_g \cdot (T - T_g) \quad \text{for } T < T_g\,. \tag{13b}$$

The temperature distribution in a sphere cooled symmetrically from the surface is given by [16]

$$T(r,t) = T_C + 2\,Bi(T_0 - T_C)\,r^{-1} \sum A_n \exp(-\delta_n\,t) \cdot \sin(\alpha_n\,r) \quad (14)$$

with $A_n = \dfrac{[\alpha_n^2 + (Bi-1)^2]\sin\alpha_n}{\alpha_n^2\,[\alpha_n^2 + Bi\,(Bi-1)]}$ and $\delta_n = [k/(c\varrho R^2)]\,\alpha_n^2$.

7.3 Calculation of permanent strains

The viscous shear strain, γ_v, is a function of both time t and position r. Since the location of freezing front, r_f, is a monotonic function of time, it can be used as a time scale. Thus

$$\gamma_v(r,t) = \gamma_v[r, t(r_f)] = \gamma_v(r, r_f)\,. \quad (15)$$

The viscous strain in a layer $r < r_f$ changes with the advancement of the freezing front until the freezing front arrives at r. Once this layer is frozen, there can be no further viscous flow and no change in the viscous strain. This frozen-in viscous strain is called the permanent (or residual) strain, γ_P. It is, as defined below, a function of r only, i.e.

$$\gamma_P(r) = \gamma_v(r, r_f)\,, \quad \text{at } r_f = r\,, \quad (16a)$$

$$\gamma_P(r) = \gamma_v(r, r)\,. \quad (16b)$$

The elastic shear strain is zero in the liquid core. So, using equations (10, 11 and 16a and b), one obtains the following expression for residual shear strain:

$$\gamma_P(r) = \frac{1}{r^3}\int_0^r (r')^3\,\frac{d\varepsilon_{th}(r', r)}{dr'}\,dr'\,. \quad (17)$$

7.4 Calculation of transient and residual stresses

In the frozen shell, elastic shear strains and stresses are calculated from known values of the auxiliary and residual shear strains.

$$\gamma_e(r, r_f) = \frac{\gamma_{aux}(r, r_f) - \gamma_p(r, r_f)}{1 + \dfrac{4\,G}{3\,K}} \quad (18a)$$

and

$$\sigma_r(r, r_f) - \sigma_\theta(r, r_f) = \tau(r, r_f) = 2\,G\,\gamma_e(r, r_f)\,. \quad (18b)$$

In the liquid core, stresses are hydrostatic and uniform. Thus,

$$\sigma_\theta(r, r_f) = \sigma_r(r, r_f) = \sigma_r(r_f, r_f)\,. \quad (18c)$$

When the whole sphere is again isothermal, at room temperature, the thermal strain gradient is zero. Therefore, the auxiliary shear strain is also zero (equation (11)). The permanent elastic shear strains and stresses are then given by

$$\gamma_{P,e}(r) = -\frac{\gamma_p(r)}{1 + \dfrac{4\,G}{3\,K}} \quad (19a)$$

and

$$\tau_P(r) = 2\,G\,\gamma_{P,e}(r)\,. \quad (19b)$$

Radial stresses, both transient and permanent, are obtained by substitution for shear stress in equation (3) followed by numerical integration.

0598P003

Addresses of the authors:

O. S. Narayanaswamy
26610 Hass Avenue
Dearborn Heights, MI 48127 (USA)

R. Gardon
28405 Eastbrook Court
Farmington Hills, MI 48334 (USA)